Common-Origin Approach to Assess Level-Ground Liquefaction Susceptibility and Triggering in CPT-Compatible Soils Using Δ_Q

Steven R. Saye, M.ASCE[1]; Scott M. Olson, M.ASCE[2]; and Kevin W. Franke, M.ASCE[3]

Abstract: Current engineering practice employs clean sand–based procedures to evaluate liquefaction triggering in nonplastic, coarse-grained soils and low-plasticity, fine-grained soils below level or mildly-sloping ground. Furthermore, existing empirical liquefaction triggering procedures treat all clean sands (fines content <5%) as identical (i.e., employing a single liquefaction resistance boundary). To improve these practices, this paper presents a new Δ_Q common-origin method to assess level-ground liquefaction susceptibility and triggering for cone penetration test (CPT)–compatible soils ranging from nonsensitive clays to clean sands using the soil classification index Δ_Q (described elsewhere). This procedure was developed using 401 documented case records of liquefaction and nonliquefaction in clean sands, silty sands, sandy silts, and low-plasticity fine-grained soils combined into a single data set. Importantly, the proposed procedure implicitly couples the evaluation of liquefaction susceptibility and triggering and does not require estimating fines content or converting measured CPT tip resistance to an equivalent clean-sand value. Rather, the proposed procedure yields unique estimates of liquefaction resistance for soils based on compressibility (as reflected in Δ_Q) such that factors that affect penetration resistance (e.g., mineralogy, grain shape, density, overconsolidation) are incorporated. The new deterministic and probabilistic procedures are illustrated using examples of liquefaction and no liquefaction in clean sands, silty sands to sandy silts, and low-plasticity fine-grained soils. **DOI: 10.1061/(ASCE)GT.1943-5606.0002515.**

Author keywords: Cone penetration test; Soil classification assessment; Liquefaction triggering; Seismic liquefaction; Earthquakes.

Introduction

The assessment of seismic liquefaction of level and mildly-sloping ground using in situ penetration tests largely is based on the pioneering work by Seed and Idriss (1971) and Whitman (1971). Seed and Idriss (1971) proposed a simplified equation to estimate seismic demand in terms of a cyclic shear stress ratio (CSR) for level-ground sites that did and did not manifest liquefaction features. They compared this seismic demand to the resistance of the soil to cyclic loading, which was characterized using relative density. A boundary that separates liquefied from not liquefied sites defines the level-ground liquefaction resistance, or cyclic resistance ratio (CRR), of sandy soils. Since 1971, numerous investigators (e.g., Seed and Idriss 1982; Seed et al. 1985; Youd et al. 2001; Cetin et al. 2004; Boulanger and Idriss 2012, among others) have expanded the case history database and refined this method to estimate CSR corresponding to a moment magnitude (M) 7.5 earthquake ($CSR_{7.5}$) and have used overburden stress-normalized standard penetration test (SPT) blow count $[(N_1)_{60}]$ to define the cyclic resistance ratio to a M7.5 earthquake ($CRR_{7.5}$).

Robertson and Campanella (1985) and Seed and de Alba (1986) extended the cyclic stress approach by defining $CRR_{7.5}$ using overburden stress-normalized cone penetration test (CPT) tip stress, q_{c1}. These early efforts differentiated soil type using measured fines content (FC) and/or median grain diameter (D_{50}). Stark and Olson (1995), Robertson and Wride (1998), Moss et al. (2006), Boulanger and Idriss (2016), and others developed similar liquefaction resistance boundaries using CPT data and variably-interpreted case history records. Fig. 1(a) presents the Robertson and Wride (1998) liquefaction resistance boundaries for sandy soils with soil behavior type index, I_c, values of 1.64, 2.07, and 2.59 corresponding to approximate $FC \approx 5\%$, 15%, and 35%.

In contrast to these in situ methods developed for coarse-grained soils, evaluating liquefaction triggering in low-plasticity fine-grained soils has been more challenging. Engineers have long recognized that saturated, fine-grained soils can indeed experience incremental excess porewater pressure generation and strain softening (or strength loss) when subjected to cyclic loading (often termed *cyclic softening*), and cases where low-plasticity, saturated, fine-grained soils have manifested consequences of liquefaction-like behavior have been reported in the literature (e.g., Bray and Sancio 2006). The susceptibility of fine-grained soils to cyclic softening and liquefaction historically has been assessed using index properties to describe soil water content (w) and/or plasticity (liquid limit, w_L, and plasticity index, I_p) by relating these index properties to observed case histories that did and did not manifest liquefaction effects. These methods originated with the Chinese criteria (described by Seed and Idriss 1982) and subsequently have been refined by several researchers (e.g., Seed et al. 2003; Boulanger and Idriss 2004, 2006; Bray and Sancio 2006).

[1]Senior Geotechnical Engineer, Kiewit Engineering Group, Inc., 1550 Mike Fahey St., Omaha, NE 68102. Email: steve.saye@kiewit.com

[2]Professor, Dept. of Civil and Environmental Engineering, Univ. of Illinois at Urbana-Champaign, 2230d Newmark Civil Engineering Laboratory, Urbana, IL 61801 (corresponding author). ORCID: https://orcid.org/0000-0002-0828-0719. Email: olsons@illinois.edu

[3]Associate Professor, Dept. of Civil and Environmental Engineering, 430J Engineering Bldg., Brigham Young Univ., Provo, UT 84602. Email: kevin_franke@byu.edu

Note. This manuscript was submitted on April 17, 2020; approved on January 13, 2021; published online on May 6, 2021. Discussion period open until October 6, 2021; separate discussions must be submitted for individual papers. This paper is part of the ***Journal of Geotechnical and Geoenvironmental Engineering***, © ASCE, ISSN 1090-0241.

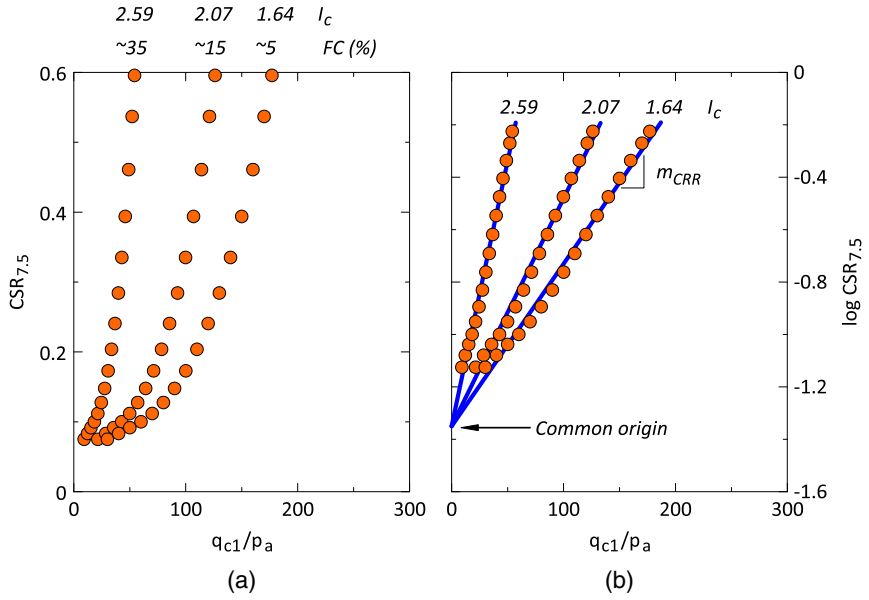

Fig. 1. (a) Liquefaction resistance boundaries proposed by Robertson and Wride (1998) for $I_c = 1.64$, 2.07, and 2.59; and (b) liquefaction resistance boundaries replotted in $q_{c1}/p_a - \log CSR_{7.5}$ space to illustrate definitions of common origin and m_{CRR}. (Data from Robertson and Wride 1998.)

In addition to navigating the differences in evaluating liquefaction susceptibility of fine-grained soils, evaluating triggering in susceptible fine-grained soils has been more contentious and potentially confusing, in part because it often is not apparent when a fine-grained soil can experience liquefaction and the subsequent undesirable consequences. Many engineers may not understand when (or even if) it is appropriate to evaluate liquefaction triggering in a susceptible fine-grained soil using in situ methods developed specifically for coarse-grained soils. For example, Boulanger and Idriss (2006) suggested that fine-grained soils with plasticity indices (I_P) less than 7 can be evaluated using in situ methods developed for coarse-grained soils, but also cautioned that fine-grained soils with I_P as low as 3–6 may exhibit intermediate behavior where more detailed in situ and cyclic laboratory testing may be needed. Similarly, Bray and Sancio (2006) recommended that fine-grained soils classified as *susceptible* or *moderately susceptible* to liquefaction based on index properties should be evaluated further using laboratory cyclic shear tests performed on undisturbed samples.

Higher plasticity fine-grained, nonsensitive soils also can experience cyclic softening, but strength loss associated with cyclic loading of high-plasticity, fine-grained, nonsensitive soils typically is less than 20% (Boulanger and Idriss 2004; Ajmena et al. 2019), and reported cases of manifestations of level-ground liquefaction (soil boils, settlement, lateral spreading) are relatively rare. In contrast, sensitive fine-grained soils (e.g., quick clays of Eastern Canada and Scandinavia) can experience severe undrained strength loss and manifest liquefaction-like features under level ground when subjected to modest static or cyclic loads. These high-sensitivity soils are not considered in this study.

In this paper, we propose a unified method to assess level-ground liquefaction susceptibility and triggering for CPT-compatible soils ranging from nonsensitive clays to clean sands using the soil classification index, Δ_Q (Saye et al. 2017). This new method (1) eliminates the need for a fines-content adjustment to adjust the CPT tip resistance measured in silty sands to an equivalent clean-sand CPT tip resistance; (2) incorporates case histories involving low-plasticity, nonsensitive fine-grained soils into the database and, in doing so, extends and unifies the evaluation of liquefaction susceptibility and triggering for coarse-grained and low-plasticity, nonsensitive fine-grained soils; and (3) differentiates the liquefaction resistance of clean sands based on CPT measurements (which reflect properties such as compressibility and mineralogy) rather than treating all clean sands identically. In the proposed framework, a common origin is defined by replotting traditional liquefaction resistance boundaries [e.g., Fig. 1(a)] in $\log_{10} CSR_{7.5} - q_{c1}/p_a$ space (where p_a is atmospheric pressure) to develop a series of linear liquefaction resistance boundaries that project to a common y-intercept (or common origin).

Using the common-origin framework, 401 liquefaction case records from a wide variety of original and secondary sources, representing 24 earthquakes ranging in moment magnitude from 5.5 to 9.0, were compiled and replotted using transformed axes to develop deterministic and probabilistic liquefaction resistance boundaries. Two sites, one where an inclinometer was installed prior to earthquake shaking and one where liquefaction-induced silt boils were manifest, are used to illustrate the application of the Δ_Q common-origin method to assess liquefaction triggering in individual soil layers ranging from clean sand to low-plasticity, nonsensitive silty clay. Additional examples are presented in the Supplemental Materials. Lastly, the authors illustrate aspects of the Δ_Q common-origin method for two particular subsets of the case history database: (1) the Darfield/Christchurch, New Zealand, cases (Green et al. 2014) for which existing liquefaction triggering methods have been only moderately successful in forecasting the observed liquefaction manifestations; and (2) cases involving low-plasticity, nonsensitive fine-grained soils where existing liquefaction triggering methods developed for coarse-grained soils do not apply.

The Common Origin

Robertson and Wride (1998) developed CPT-based liquefaction resistance boundaries for sandy soils as part of the National Center for Earthquake Engineering Research (NCEER) study that culminated in the level-ground liquefaction triggering assessment guidelines summarized by Youd et al. (2001). The three liquefaction resistance

Table 1. Common-origin $\log_{10}CRR_{7.5}$ intercepts for several published CPT-based liquefaction resistance boundaries

Reference	Common-origin $CRR_{7.5}$ intercept, c_o
Stark and Olson (1995)	−1.30
Robertson and Wride (1998)	−1.35
Moss et al. (2006)	−1.39
Boulanger and Idriss (2016)	−1.22

boundaries for $FC \approx 5\%$, 15%, and 35% [Fig. 1(a)] are replotted in $\log_{10}CRR_{7.5} - q_{c1}/p_a$ space in Fig. 1(b). As illustrated in the figure, when plotted in $\log_{10}CRR_{7.5} - q_{c1}/p_a$ space, the Robertson and Wride (1998) boundaries can be approximated as straight lines that converge to a common origin of $\log_{10} CRR_{7.5} = -1.35$ at $q_{c1}/p_a = 0$. Table 1 summarizes common-origin $\log_{10} CRR_{7.5}$ intercepts derived from other published CPT-based liquefaction resistance boundaries. As detailed subsequently, statistical regression using the liquefaction and nonliquefaction case history data set introduced later in this paper (Table S1) yielded a common origin of $\log_{10} CRR_{7.5} = -1.34$.

As illustrated in Fig. 1(b), each boundary exhibits a unique slope, defined as m_{CRR}, which is expressed as

$$m_{CRR} = \frac{\log_{10}CRR_{7.5} - c_o}{\frac{q_{c1}}{p_a}} \quad (1)$$

where c_o = value of the common origin for $CRR_{7.5}$ (i.e., the $\log_{10}CRR_{7.5}$-axis intercept at $q_{c1}/p_a = 0$). Slopes of m_{CRR} can be related to soil-type indices such as D_{50} or FC, as shown in Figs. 2(a and b), respectively. Similarly, Fig. 2(c) shows that m_{CRR} values for the Robertson and Wride (1998) boundaries can be related to the Robertson and Wride (1998) soil behavior type index, I_c.

As illustrated in Figs. 1(b) and 2, each liquefaction resistance boundary involves three variables: (1) $\log_{10}CRR_{7.5}$, which characterizes seismic demand required to trigger liquefaction; (2) q_{c1}/p_a, which characterizes soil resistance to seismic loading; and (3) a parameter describing soil type or behavior (e.g., FC, D_{50}, I_c). Other CPT-based triggering approaches (e.g., Moss et al. 2006; Boulanger and Idriss 2016) eliminate one variable by using an empirical fines-content adjustment ($\Delta q_{c1}/p_a$) to adjust the q_{c1}/p_a measured in silty sands to equivalent values consistent with clean sands [$(q_{c1})_{cs}/p_a$], thereby yielding a single clean-sand liquefaction resistance boundary relating $CRR_{7.5}$ and $(q_{c1})_{cs}/p_a$. These adjustments tend to be highly uncertain, in part because they depend on both FC and q_{c1}/p_a. Furthermore, these adjustments may not account for the plasticity and other characteristics of the fines, which can affect liquefaction resistance. Lastly, the use of a single clean-sand liquefaction boundary does not account for potential variations in q_{c1}/p_a that occur in clean sands with different fabric compressibility and/or grain mineralogy (e.g., Robertson and Campanella 1983).

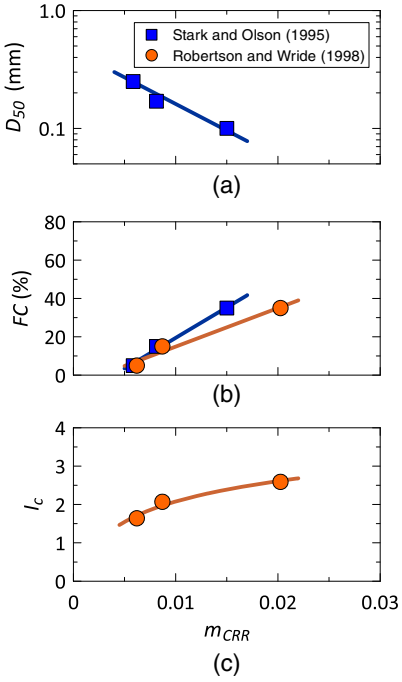

Fig. 2. Trends of soil indices with m_{CRR}: (a) D_{50} (mm); (b) FC (%); and (c) I_c.

In this paper, we combine the seismic demand required to trigger liquefaction and the soil's resistance to liquefaction into a single term, m_{CRR}. To characterize soil type or behavior for liquefaction triggering assessment, we use the soil classification index Δ_Q (Saye et al. 2017), which implicitly is affected by geotechnical properties such as plasticity, compressibility, and grain size distribution. Thus, the proposed Δ_Q common-origin approach (1) eliminates the need for an equivalent clean-sand adjustment or an estimate of FC from the CPT (i.e., the fines-content adjustment, $\Delta q_{c1}/p_a$) used by all other CPT-based liquefaction triggering approaches for sandy soils; (2) extends CPT-based liquefaction triggering to clayey soils such that all CPT-compatible soils ranging from nonsensitive clays to clean sands can be evaluated using a single, unified susceptibility and triggering procedure; and (3) accommodates variations in the liquefaction resistance of clean sands with different fabric compressibility and/or grain mineralogy.

Soil Classification Using Δ_Q

Saye et al. (2017) presented an empirical assessment of soil classification using CPT data in $Q_t - f_s/\sigma'_{v_0}$ space, where $Q_t = (q_t - \sigma_{v_0})/\sigma'_{v_0}$, q_t = corrected CPT tip stress, f_s = CPT sleeve friction, σ_{v_0} = initial total vertical stress, and σ'_{v_0} = initial effective vertical stress. Fig. 3(a) illustrates individual CPT data for different soil types interpreted in $Q_t - f_s/\sigma'_{v_0}$ space. As shown in the figure, each soil type exhibits a unique linear slope and the family of lines converge to an offset origin of $Q_t = -10$ and $f_s/\sigma'_{v_0} = -0.67$. Saye et al. (2017) defined the slope of each set of CPT data as Δ_Q, which is expressed as

$$\Delta_Q = \frac{Q_t + 10}{\frac{f_s}{\sigma'_{v_0}} + 0.67} \quad (2)$$

Fig. 3(b) illustrates the resulting Δ_Q-based soil classification approach. Saye et al. (2017) showed that the linear Δ_Q relations transform into hyperbolas when plotted in $Q_t - F$ space used by Robertson (1990) [where $F = f_s/(q_t - \sigma_{v_0})$] that more effectively capture changes in soil type and stress history (i.e., overconsolidation) than I_c. By relating m_{CRR} to Δ_Q, soil-specific liquefaction resistance boundaries can be defined for all CPT-compatible soil types (from low-plasticity fine-grained to clean coarse-grained soils with differing grain mineralogy) in a manner that accounts directly for the soil properties that affect penetration resistance, porewater pressure generation, and liquefaction resistance (including plasticity, compressibility, and gradation). Thus, the proposed $m_{CRR} - \Delta_Q$ relationship presented in this paper provides unique liquefaction resistance boundaries for clean sands with different compressibility and mineralogy (i.e., low-compressibility silica sands compared to higher compressibility carbonate sands or

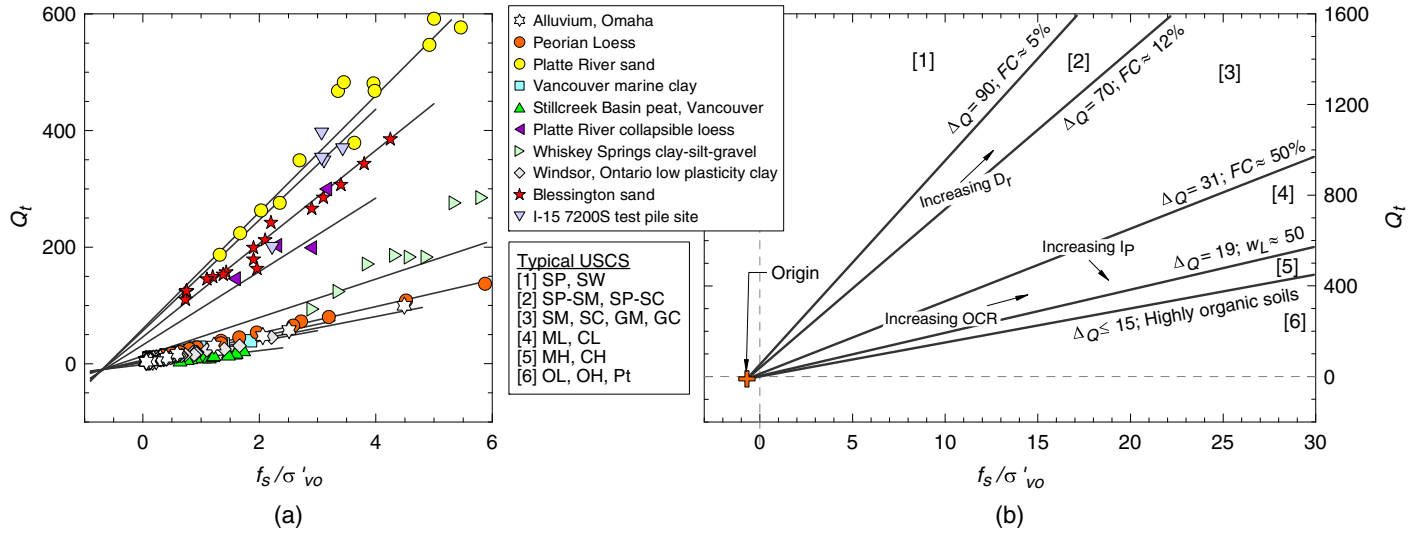

Fig. 3. (a) Relationships between f_s/σ'_{vo} and Q_t for individual soils; and (b) soil classification assessment chart using Δ_Q. USCS = Unified Soil Classification System; SP = poorly-graded sand; SW = well-graded sand; SP-SM = poorly graded sand with silt; SP-SC = poorly graded sand with clay; SM = silty sand; SC = clayey sand; GM = silty gravel; GC = clayey gravel; ML = low-plasticity silt; CL = low-plasticity clay; MH = high-plasticity (elastic) silt; CH = high-plasticity clay; OL = low-plasticity organic soil; OH = high-plasticity organic soil; and Pt = peat. (Adapted from Saye et al. 2017.)

well-graded sands compared to poorly graded sands), as well as for silty or clayey soils with differing plasticity, as these factors change the Δ_Q value for the soil.

Field Liquefaction Data Set

To create a $m_{CRR} - \Delta_Q$ relationship, a data set of vetted case histories involving a wide range of soil types where liquefaction was and was not manifest is required. Table S1 summarizes the liquefaction and nonliquefaction cases compiled to develop the proposed $m_{CRR} - \Delta_Q$ relationship in this study. To compile this data set, the authors carefully reviewed and evaluated liquefaction and nonliquefaction cases reported in a wide variety of original and secondary sources, involving 24 earthquakes with moment magnitudes ranging from 5.5 to 9.0. Cases involving marginal liquefaction (i.e., reported by the original investigators as "minor," "sparse," or "marginal" surface manifestations) are identified in the table. Importantly, in contrast to previous investigators we did not differentiate sandy soil case histories from clayey soil case histories. All field data, from clayey to sandy soils, were processed uniformly as described below.

Cyclic stress ratios normalized to a $M7.5$ earthquake ($CSR_{7.5}$) were calculated using the simplified equation (Seed and Idriss 1971; Whitman 1971) and the adjustments recommended by Youd et al. (2001). The $CSR_{7.5}$ term was defined as

$$CSR_{7.5} = \frac{CSR}{MSF} = \frac{\tau_{\text{avg}}/\sigma'_{vo}}{MSF} = \frac{0.65(\frac{a_{\max}}{g})(\frac{\sigma_{vo}}{\sigma'_{vo}})r_d}{MSF} \tag{3}$$

where MSF = magnitude scaling factor; τ_{avg} = average shear stress; $a_{\max}$ = peak ground surface acceleration; g = acceleration of gravity; and r_d = depth reduction factor. The MSF and r_d terms were defined as

$$MSF = \frac{10^{2.24}}{M^{2.56}} \tag{4}$$

and

$$r_d = \begin{cases} 1.0 - 0.00765z & \text{for } z < 9.15m \\ 1.174 - 0.0267z & \text{for } 9.15m < z < 23m \end{cases} \tag{5}$$

where z = depth below the ground surface (meters). At this time, we selected the Youd et al. (2001) recommended relationships for MSF and r_d as they are widely recognized, vetted, and still used in practice. Future iterations of the $m_{CRR} - \Delta_Q$ relationship may consider alternate MSF and r_d correlations, e.g., Cetin et al. (2004), Boulanger and Idriss (2014), and others.

The depth of the critical layers reported in Table S1 are relatively shallow, resulting in effective vertical stress corrections (K_σ) of 1.0 for the vast majority of the cases in the data set using the Youd et al. (2001) K_σ correction factor. [Here, we considered the Youd et al. (2001) K_σ correction factor to maintain a consistent, uniform data processing procedure, as we were using the Youd et al. MSF and r_d factors.] In fact, greater than 93% of the cases in the database have $\sigma'_v \le 100$ kPa and $K_\sigma = 1.0$. For comparison, approximately 90% of cases in the database have $K_\sigma = 0.98$–1.07 using the Boulanger and Idriss (2016) K_σ factor. Therefore, this study did not incorporate K_σ, which is consistent with some other previous liquefaction triggering studies (e.g., Kayen et al. 2013). Additionally, this study considers only level-ground or nearly level-ground conditions, consistent with most previously published liquefaction triggering studies; therefore, the static shear stress adjustment (K_α) was not included in this study. Again, future iterations of the $m_{\text{CRR}} - \Delta_Q$ relationship may consider alternate K_σ and K_α correlations, e.g., Cetin et al. (2004) and Boulanger and Idriss (2014).

Dimensionless CPT tip stress was computed as follows:

$$\frac{q_{c1}}{p_a} = C_q\left(\frac{q_c}{p_a}\right) \tag{6}$$

where

$$C_q = \left(\frac{p_a}{\sigma'_{v0}}\right)^n \le 1.7 \tag{7}$$

and n was defined as 0.5, regardless of soil type. We opted to not use the Robertson (2009) approach (or similar alternate approaches) to calculate q_{c1N} based on variations in I_c and instead computed the dimensionless q_{c1}/p_a using a single value of the exponent $n = 0.5$ to focus on the soil-type variations related to Δ_Q [computed using Eq. (2)].

Much of the CPT data from legacy liquefaction case histories in the literature report only q_c rather the tip stress corrected for unequal end area effects, q_t. Furthermore, penetration-induced porewater pressures were measured for only a fraction of the cases in Table S1. Therefore, we elected to process all data as q_c, concluding that uniform and consistent data processing was more important than the improved characterization of the fine-grained soils with q_t. We note that the critical layer mid-depths reported in Table S1 are generally shallow (~70% are <5 m and ~95% are <8 m). At these shallow depths, considering a groundwater depth of 1 m and typical values of penetration-induced excess porewater pressure (Δu_2) for soft, nearly normally consolidated fine-grained soils (e.g., Robertson and Cabal 2015), the difference in Δ_Q computed from q_c and q_t is less than 5%. These small differences in Δ_Q have a negligible effect on the Δ_Q common-origin approach presented here. Future iterations of the $m_{CRR} - \Delta_Q$ relationship may consider developing a general approach to correct historical q_c data to equivalent q_t values, but such an effort was not attempted at this time.

Selecting Critical Layers for the Δ_Q Common-Origin Approach

Recent level-ground liquefaction triggering data sets (e.g., Moss et al. 2006; Green et al. 2014; Boulanger and Idriss 2016) identify a potential critical soil layer and *typically* (but not always) report average q_c and f_s values within this layer. In contrast, $CSR_{7.5}$ values *typically* are reported for the mid-depth of the critical layer. When developing conventional liquefaction resistance boundaries, this intermingling of average CPT values (which typically do not occur at the layer mid-depth) and mid-depth $CSR_{7.5}$ values likely has a minor effect on the resulting boundary. However, in the Δ_Q common-origin approach, the m_{CSR} term [where $m_{CSR} = (\log_{10} CSR_{7.5} - c_o)/(q_{c1}/p_a)$] includes both $CSR_{7.5}$ and q_{c1}/p_a. When these values do not correspond to the same specific depth, the computed m_{CSR} value does not correspond to the depth of either $CSR_{7.5}$ or q_{c1}, and therefore is incorrect. Similarly, when average q_c and f_s values (which typically do not occur at the layer mid-depth) are combined with the mid-depth σ'_v value to compute Δ_Q, the resulting Δ_Q value differs from the value that would be defined if Δ_Q were averaged over the layer. Thus, we computed Δ_Q and m_{CSR} for each depth in a sounding, and we then reported in Table S1 average values within the selected critical layer for all relevant CPT and seismic parameters.

To select (or verify) the critical layer for each liquefaction case history in Table S1, we typically identified two depth ranges: (1) the broader sediment (or stratigraphic/geologic) unit that contains the critical layer; and (2) the critical layer which represents the weakest-link-in-the-chain zone within the sediment unit. This differentiation is important when variations occur within the sediment unit, and the approach aligns with the recommendations in the National Academies (2016) study on the state of the art and practice in liquefaction assessment. Specifically, we consistently identified the critical layer (within the sediment unit) as the shallowest soil layer that is both susceptible to liquefaction and most likely to develop surface manifestations at a liquefaction site. At a nonliquefaction site, the critical layer was defined as the layer that is most susceptible to liquefaction and could most likely result in at least minor surface manifestations if triggered to liquefy (Green et al. 2014). As noted by Green et al. (2014), the critical layer needs to satisfy the depth-thickness-density concepts defined by Olson et al. (2005) and Green et al. (2005) and be consistent with the observed surface evidence of liquefaction at the site (e.g., soil composition, grain size, and color of the observed ejecta).

Therefore, our selection and/or verification of the critical layer for each case history consistently considered the following: (1) similarity in grain size distribution with documented ejecta (where available); (2) depth of the critical layer relative to the a low-permeability confining layer (e.g., clay cap or asphalt pavement) for cases of hydraulic fracturing; (3) spatial continuity of the critical layer (i.e., similar soil type, elevation, and penetration resistance) over the extent of the surface manifestations for cases of lateral spreading; (4) depth of the critical layer relative to the base of a free-face (as appropriate) in cases of lateral spreading; (5) observations from nearby inclinometers, piezometers, or other instrumentation (where available); and (6) depth of the critical layer relative to building foundations in cases of observed postliquefaction building settlement or tilting.

To illustrate how critical layers were evaluated and identified consistently for all of the case histories in Table S1, we present four examples that illustrate the (1) use of specific instrumentation data to subdivide a sediment unit into multiple critical layers; (2) selection of a shallower potentially liquefiable layer as critical; (3) minor revision of critical layer depth limits to be more consistent with specific CPT measurements; and (4) identification of a weakest-link-in-the-chain critical layer within a sediment unit. Examples 1–3 are presented in the Supplemental Materials, and Example 4 is presented below.

Fig. 4 presents data from CPT sounding LEN-37 conducted at the Leonardini Farm site following the 1989 Loma Prieta earthquake (Bennett and Tinsley 1995; Charlie et al. 1998). Extensive cracking parallel to the riverbank and displacements of up to 2 m occurred near the toe of the lateral spread at this site. Boulanger and Idriss (2016) identified a critical layer between 2.5 and 7.5 m, with a reported average depth of 4.9 m. As illustrated in Fig. 4, a *sand with silt* sediment unit (as identified by both measured fines content and Δ_Q) occurs from 2.5 to 7.7 m in this sounding, so the authors extended this sediment unit to a depth of 7.7 m for this sounding. However, at this site the upper portion of the sand with silt unit (2.5–5.0 m; $\Delta_Q \approx 75$) exhibits a nontrivial difference in Δ_Q compared to the lower portion of the unit (5.0–7.7 m; $\Delta_Q \approx 62$). Therefore, using the selection rules described previously, we selected the upper portion of the sand with silt sediment unit (2.5–5.0 m; $\Delta_Q \approx 75$) as the critical layer.

Development of m_{CRR} Model

Fig. 5 presents the revised liquefaction, marginal liquefaction, and nonliquefaction case history data from Table S1 in both arithmetic and log-log $m_{CSR} - \Delta_Q$ space. As noted previously, a common origin (c_o) of −1.34 was computed in this study through statistical regression. Visual inspection of Fig. 5 reveals a separation between liquefaction and nonliquefaction case histories as a function of Δ_Q, with marginal liquefaction data generally plotting near the visual boundary between the liquefaction and nonliquefaction cases. In $m_{CSR} - \Delta_Q$ space, the boundary between the liquefaction and nonliquefaction cases is, by definition, m_{CRR}. Based on the data in Table S1, we computed the most likely location of this boundary (i.e., the m_{CRR} model) using Bayesian updating and maximum likelihood estimation (MLE) techniques. This regression is detailed

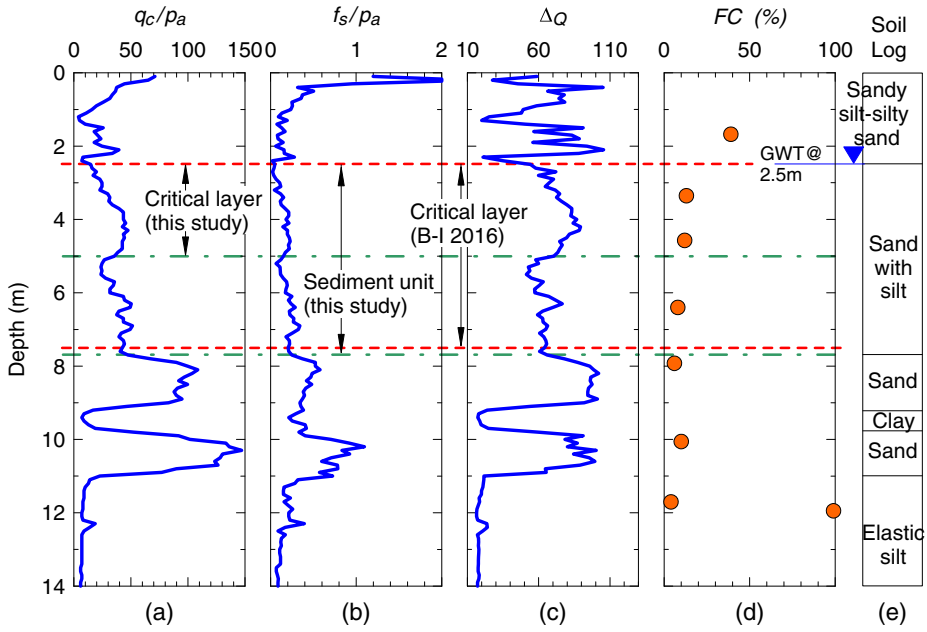

Fig. 4. Summary of Leonardini Farm site CPT sounding LEN-37: (a) dimensionless tip resistance; (b) dimensionless sleeve friction; (c) Δ_Q soil classification index; (d) fines content; and (e) soil log. Included in the figure are the critical layer used by Boulanger and Idriss (2016) and the sediment unit and critical layer used in this study.

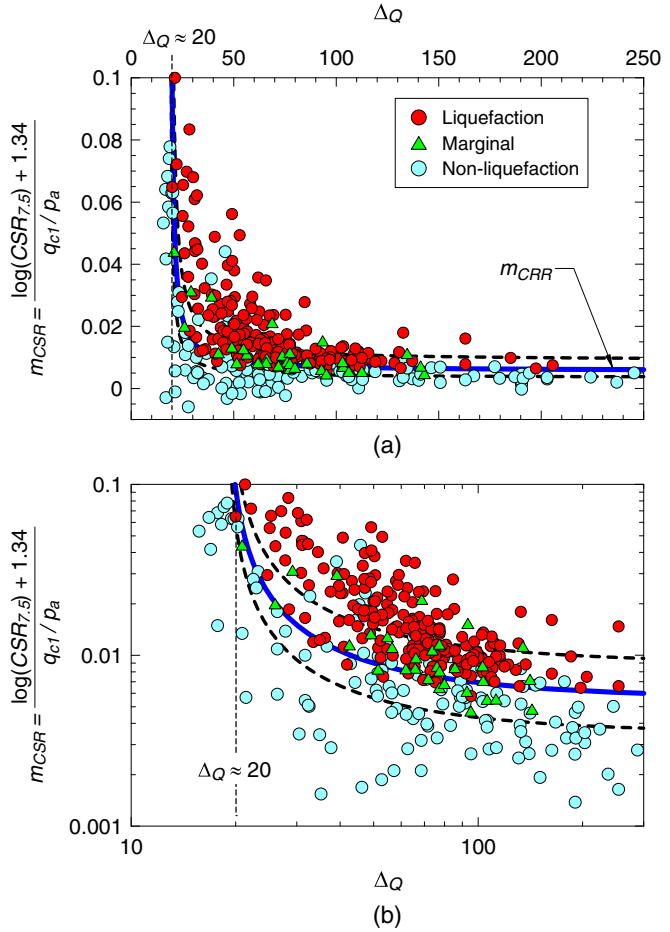

Fig. 5. $\hat{m}_{CRR}$ and $\hat{m}_{CRR} \pm 1\sigma$ plotted with liquefaction, marginal liquefaction, and nonliquefaction case histories from Table S1: (a) arithmetic scale; and (b) log-log scale.

thoroughly in the Supplemental Materials. The following summarizes the regression procedure and analysis results.

Bayesian updating is based on a framework for estimating unknown model parameters, given as

$$f(\Theta) = cL(\Theta)p(\Theta) \tag{8}$$

where Θ = set of model parameters to be estimated; $p(\Theta)$ = existing probability distribution representing our knowledge about Θ prior to adding additional observations; $L(\Theta)$ = likelihood function representing our new knowledge gained from a set of new observations; $c = [\int L(\Theta)p(\Theta)d\Theta]^{-1}$ is a normalization factor; and $f(\Theta)$ = posterior distribution representing our updated state of knowledge about Θ (Box et al. 1973; Der Kiureghian 1999; Cetin et al. 2002).

Limit State Function

A limit state function was developed to represent the boundary between liquefaction and nonliquefaction case histories in $m_{CSR} - \Delta_Q$ space. This model is used in the Bayesian updating approach to regress the most likely model coefficients for m_{CRR} given the current case history data. Such limit state functions have been applied by other researchers to develop probabilistic liquefaction triggering models (e.g., Liao et al. 1988; Liao and Lum 1998; Youd and Noble 1997; Cetin et al. 2004; Boulanger and Idriss 2012).

Consistent with Boulanger and Idriss (2012), the following notation was used for convenience to develop the limit state function:

$$q = \frac{q_{c1}}{p_a} \tag{9}$$

$$S = CSR_{7.5} \tag{10}$$

$$m_R = m_{CRR} \tag{11}$$

$$m_S = m_{CSR} \tag{12}$$

J. Geotech. Geoenviron. Eng., 2021, 147(7): 04021046

The limit state function, including uncertainties, then is formulated as follows:

$$g(q, \Delta_Q, S, \mathbf{C}) = \ln(m_R) - \ln(m_S) \tag{13}$$

$$g(q, \Delta_Q, S, \mathbf{C}) = \ln\left[\frac{\Delta_Q}{C_1 \cdot \Delta_Q + C_2}\right] - \ln\left[\frac{\log S + C_3}{q}\right] \tag{14}$$

$$g(q, \Delta_Q, S, \mathbf{C}) = \ln\left[\frac{\hat{\Delta}_Q}{C_1 \cdot \hat{\Delta}_Q + C_2}\right] - \ln\left[\frac{\log \hat{S} + C_3}{\hat{q}}\right] + \varepsilon \tag{15}$$

where $\mathbf{C}$ = vector representing unknown coefficients C_1–C_3; and ε = total uncertainty. Note that ε could be broken further into its component contributions from Δ_Q, S, and q. However, such detail is not necessary for the m_R function at this stage, because Eq. (15) is only an intermediate function in computing the probability of liquefaction and/or the factor of safety against liquefaction triggering. Parametric uncertainties in S and q will be considered later in the formulation of the liquefaction resistance boundary. Finally, use of the hat terms in Eq. (15) indicate median values of their associated parameters.

For case histories exhibiting liquefaction manifestations (i.e., $g \leq 0$), the probability of observing liquefaction is computed as

$$P[g(q, \Delta_Q, S, \mathbf{C}) \leq 0] = \Phi\left[-\frac{g(\hat{q}, \hat{\Delta}_Q, \hat{S}, \mathbf{C})}{\sigma_{\ln m_R}}\right] \tag{16}$$

where Φ = standard normal cumulative probability distribution function. For case histories showing no liquefaction manifestations (i.e., $g > 0$), the probability of observing no liquefaction is computed as

$$P[g(q, \Delta_Q, S, \mathbf{C}) > 0] = \Phi\left[\frac{g(\hat{q}, \hat{\Delta}_Q, \hat{S}, \mathbf{C})}{\sigma_{\ln m_R}}\right] \tag{17}$$

The likelihood function then can be written as

$$L(\mathbf{C}, \varepsilon) = \prod_{\text{Liquefied Sites}} P[g(q, \Delta_Q, S, \mathbf{C}) \leq 0] \times \prod_{\text{Nonliquefied Sites}} P[g(q, \Delta_Q, S, \mathbf{C}) > 0] \tag{18}$$

$$L(\mathbf{C}, \varepsilon) = \prod_{\text{Liquefied Sites}} \Phi\left[-\frac{g(\hat{q}, \hat{\Delta}_Q, \hat{S}, \mathbf{C})}{\sigma_{\ln m_R}}\right] \times \prod_{\text{Nonliquefied Sites}} \Phi\left[\frac{g(\hat{q}, \hat{\Delta}_Q, \hat{S}, \mathbf{C})}{\sigma_{\ln m_R}}\right] \tag{19}$$

where Π = product of the sequence of terms.

Correcting for Sampling Bias

Cetin et al. (2002) suggested that uneven sampling in liquefaction/nonliquefaction case histories can potentially bias the maximum likelihood results. As cited by both Cetin et al. (2002) and Boulanger and Idriss (2012), Manski and Lerman (1977) suggested that the bias from an uneven choice-based sampling process could be corrected by weighting the observations to better represent the actual population. Rewriting Eq. (19) to correct for this bias, the modified likelihood function is given as

$$L(\mathbf{C}, \varepsilon) = \prod_{\text{Liquefied Sites}} \Phi\left[-\frac{g(\hat{q}, \hat{\Delta}_Q, \hat{S}, \mathbf{C})}{\sigma_{\ln m_R}}\right]^{w_{\text{liquefied}}} \times \prod_{\text{Nonliquefied Sites}} \Phi\left[\frac{g(\hat{q}, \hat{\Delta}_Q, \hat{S}, \mathbf{C})}{\sigma_{\ln m_R}}\right]^{w_{\text{nonliquefied}}} \tag{20}$$

where $w_{\text{liquefied}}$ and $w_{\text{nonliquefied}}$ = exponents used to weight the likelihood function. These exponents could theoretically be computed as

$$w_{\text{liquefied}} = \frac{Q_{\text{liq,true}}}{Q_{\text{liq,sample}}} \tag{21}$$

$$w_{\text{nonliquefied}} = \frac{1 - Q_{\text{liq,true}}}{1 - Q_{\text{liq,sample}}} \tag{22}$$

where $Q_{\text{liq,true}}$ = true proportion of occurrences of liquefaction in the population; and $Q_{\text{liq,sample}}$ = proportion of occurrences of liquefaction in the sample set. However, $Q_{\text{liq,true}}$ is unknown.

Cetin et al. (2002) relied upon an expert panel to develop estimates of $w_{\text{liquefied}}$ and $w_{\text{nonliquefied}}$. The panel agreed that the ratio of $w_{\text{liquefied}}/w_{\text{nonliquefied}}$ should be between 1.0 and 3.0, with the most common estimate being between 1.5 and 2.0. Cetin et al. (2004), Moss et al. (2006), and Boulanger and Idriss (2012, 2016) adopted a $w_{\text{liquefied}}/w_{\text{nonliquefied}}$ ratio of 1.5, with $w_{\text{liquefied}} = 0.8$ and $w_{\text{nonliquefied}} = 1.2$. However, the case histories presented in Table S1 include a significantly larger number of nonliquefaction case histories [liquefaction/nonliquefaction, L/N, ratio of 252/149, compared to ratios of 139/43 and 182/71 for CPT-based databases from Moss et al. (2006) and Boulanger and Idriss (2016), respectively], thus effectively reducing the sampling bias in the data set. Based on the ratio of liquefaction to nonliquefaction case histories presented in the data set, we have adopted a $w_{\text{liquefied}}/w_{\text{nonliquefied}}$ ratio of 1.22, with $w_{\text{liquefied}} = 0.9$ and $w_{\text{nonliquefied}} = 1.1$. Note that this ratio remains within the range recommended by the expert panel described by Cetin et al. (2002).

Results

The likelihood function in Eq. (20) was solved using MLE regression with the case history data presented in Table S1 to find the most likely values for C_1–C_3 and $\sigma_{\ln m_R}$. These values are presented in Table 2. Using these coefficients, the median function for m_{CRR} (i.e., 50th percentile) is given as

$$\hat{m}_{CRR} = \frac{\hat{\Delta}_Q}{178(\hat{\Delta}_Q) - 3{,}349} \leq 0.1 \quad \text{for } \Delta_Q \geq 20 \tag{23}$$

Fig. 5 presents the liquefaction case history data from Table S1 together with $\hat{m}_{CRR}$ (solid line) and $\hat{m}_{CRR} \pm 1\sigma$ (dashed lines). Note from Eq. (23) that the function for $\hat{m}_{CRR}$ is asymptotic at $\Delta_Q \approx 20$, implying that soils with $\Delta_Q < 20$ are generally not susceptible to liquefaction triggering, regardless of the strength of shaking.

Soil index property data presented by Saye et al. (2017) indicate that $\Delta_Q \approx 20$ corresponds approximately to $w_L \approx 30\%$–40%, $I_P \approx 15\%$–20%, and $D_{50} \approx 0.03$ mm. Therefore, this Δ_Q value

Table 2. Regressed coefficients and standard deviation for m_{CRR}

C_1	C_2	C_3	$\sigma_{ln}(mR)$
178	−3,349	1.340	0.471

J. Geotech. Geoenviron. Eng., 2021, 147(7): 04021046

marks an approximate change between low-plasticity, nonsensitive fine-grained soils susceptible to level-ground liquefaction and medium-plasticity, nonsensitive fine-grained soils and organic soils not susceptible to liquefaction (although these soils may be susceptible to minor cyclic softening). Specifically, this range of plasticity estimated from Δ_Q is (1) consistent with the transition at $I_P = 18$ from *moderate susceptibility* to *not susceptible to liquefaction* reported by Bray and Sancio (2006); (2) reasonably consistent the transition at $I_P \approx 13$–20 from significant to minor cyclic softening [i.e., when defined as the ratio of cyclic undrained shearing resistance to monotonic undrained shear strength (τ_{cyc}/s_u) at 15 cycles or 3% shear strain] from data compiled by Boulanger and Idriss (2004); and (3) reasonably consistent with the transition at $I_P \approx$ 15–25 from significant to minor cyclic softening (i.e., when defined as the ratio of postcyclic to monotonic undrained shear strength) reported by Ajmera et al. (2019). [As noted earlier, Δ_Q values for fine-grained soils in this study were computed using values of q_c rather than q_t, resulting in Δ_Q values that are slightly larger than identified by Saye et al. (2017); however, this difference will rarely exceed 5%].

Careful inspection of Fig. 5 reveals that nine nonliquefaction and five marginal liquefaction cases plot more than one standard deviation above the proposed m_{CRR} relationship, while none of the liquefaction cases plot more than ½ standard deviation below the relationship and none of the marginal liquefaction cases plot more than one standard deviation below the relationship. Most of these cases that plot more than one standard deviation above the proposed relationship involve sites with relatively thick nonliquefiable soils overlying potentially liquefiable fine-grained or coarse-grained layers. As originally suggested by Ishihara (1985) and confirmed by numerous investigators, these thick nonliquefiable soils may have prevented the manifestation of surface liquefaction features, even if the susceptible soils did liquefy. To maintain consistency in the database, we maintained the site/liquefaction designations reported by the original investigators. Further evaluation of these cases is planned.

Overall, this methodology effectively unifies liquefaction susceptibility and triggering analysis for low-plasticity, nonsensitive fine-grained soils with the traditional framework for coarse-grained soils, eliminating the need for fines-content estimates or equivalent clean-sand adjustments. However, we emphasize that the data set in Table S1 includes no cases of liquefaction or nonliquefaction involving quick clays or other potentially sensitive, meta-stable fine-grained soils. As such, the liquefaction resistance relationships proposed here should not be used with these types of soils. Future revisions of this work may incorporate such case histories in the regressed data set and resulting predictive models.

Δ_Q Common-Origin Liquefaction Triggering Evaluation

Probabilistic Liquefaction Resistance Boundaries

Based on the MLE regression results detailed in the Supplemental Materials, we recommend the following probabilistic relationship to evaluate liquefaction triggering:

$$\log_{10} CRR_{7.5} = \hat{m}_{CRR}\left(\frac{q_{c1}}{p_a}\right) - 1.34 + \sigma \cdot \Phi^{-1}[P_L] \tag{24}$$

where $\hat{m}_{CRR}$ is computed with Eq. (23) as a function of $CSR_{7.5}$ [Eq. (3)], q_{c1}/p_a [Eq. (6)], and Δ_Q [Eq. (2)]; Φ^{-1} = inverse of the standard cumulative normal distribution; P_L = probability of liquefaction; and σ = standard deviation and is equal to 0.24 if input parameters for a given soil layer are uncertain, or 0.20 if input parameters for a given soil layer are certain. For most typical engineering applications, input parameters for liquefaction triggering assessment are based on limited site exploration and laboratory testing data and therefore justify $\sigma = 0.24$. The selection of P_L in Eq. (24) is subjective and should be based on the acceptable error in assessing liquefaction triggering. The median value of $CRR_{7.5}$ corresponds to $P_L = 50\%$ and represents the 50th-percentile or best-fit boundary curve for the liquefaction, marginal liquefaction, and nonliquefaction case history data in Table S1.

Eq. (24) is limited to values of $\hat{m}_{CRR} \le 0.1$ and $q_{c1}/p_a \le 180$ based on the limitations of the empirical data represented in Table S1 and the general understanding that soil layers with $q_{c1}/p_a > 180$ are too dense to liquefy (e.g., Robertson and Wride 1998; Idriss and Boulanger 2008; among others). We emphasize that Eq. (24) should not be thought of as a two-dimensional liquefaction resistance boundary in q_{c1}/p_a–$CSR_{7.5}$ space, as it has been portrayed historically. Rather, Eq. (24) represents a three-dimensional liquefaction resistance boundary *surface* in q_{c1}/p_a–$CSR_{7.5}$–Δ_Q space, where $CRR_{7.5}$ is related to q_{c1}/p_a as a function of m_{CRR}, which is, in turn, a function of Δ_Q. Fig. 6 illustrates the resulting three-dimensional surface for $P_L = 50\%$.

Once $CRR_{7.5}$ and $CSR_{7.5}$ are computed using Eqs. (24) and (3), respectively, the factor of safety against liquefaction triggering is computed conventionally as follows:

$$FS_{liq} = \frac{CRR_{7.5}}{CSR_{7.5}} \tag{25}$$

Alternatively, liquefaction triggering can be evaluated and expressed in terms of probability of liquefaction as

$$P_L = \Phi\left[-\frac{(\hat{m}_{CRR}(\frac{q_{c1}}{p_a}) - 1.34) - \log_{10}(CSR_{7.5})}{\sigma}\right] \tag{26}$$

where $\hat{m}_{CRR}$ is computed as a function of $CSR_{7.5}$ [Eq. (3)], q_{c1}/p_a [Eq. (6)], and Δ_Q [Eq. (2)]; and, as discussed above, σ is equal to 0.24 if input parameters (i.e., cone tip resistance and $CSR_{7.5}$) are uncertain, or 0.20 if input parameters are assumed to be known with certainty.

Deterministic Liquefaction Resistance Boundary and Design Factors of Safety

Historically, liquefaction resistance boundaries (e.g., Seed et al. 1985; Robertson and Campanella 1985; Stark and Olson 1995; among others) were defined visually (i.e., deterministically), not statistically. With the introduction of statistically computed liquefaction resistance boundaries, researchers began identifying the value of P_L that corresponded to their visually determined boundary. This value of P_L has often been approximately 15% (Cetin et al. 2004; Moss et al. 2006; Boulanger and Idriss 2012, 2016).

Here, we recommend using $P_L = 35\%$ with $CRR_{7.5}$ in Eq. (24) to define a deterministic liquefaction resistance boundary for use in design. This approach shifts the liquefaction resistance boundary down by approximately one-half of a standard deviation, effectively creating a conservative boundary for liquefaction triggering assessment. Thus, for deterministic liquefaction triggering assessment, we recommend computing $CRR_{7.5}$ as

$$\log_{10} CRR_{7.5} = \hat{m}_{CRR}\left(\frac{q_{c1}}{p_a}\right) - 1.34 - X \tag{27}$$

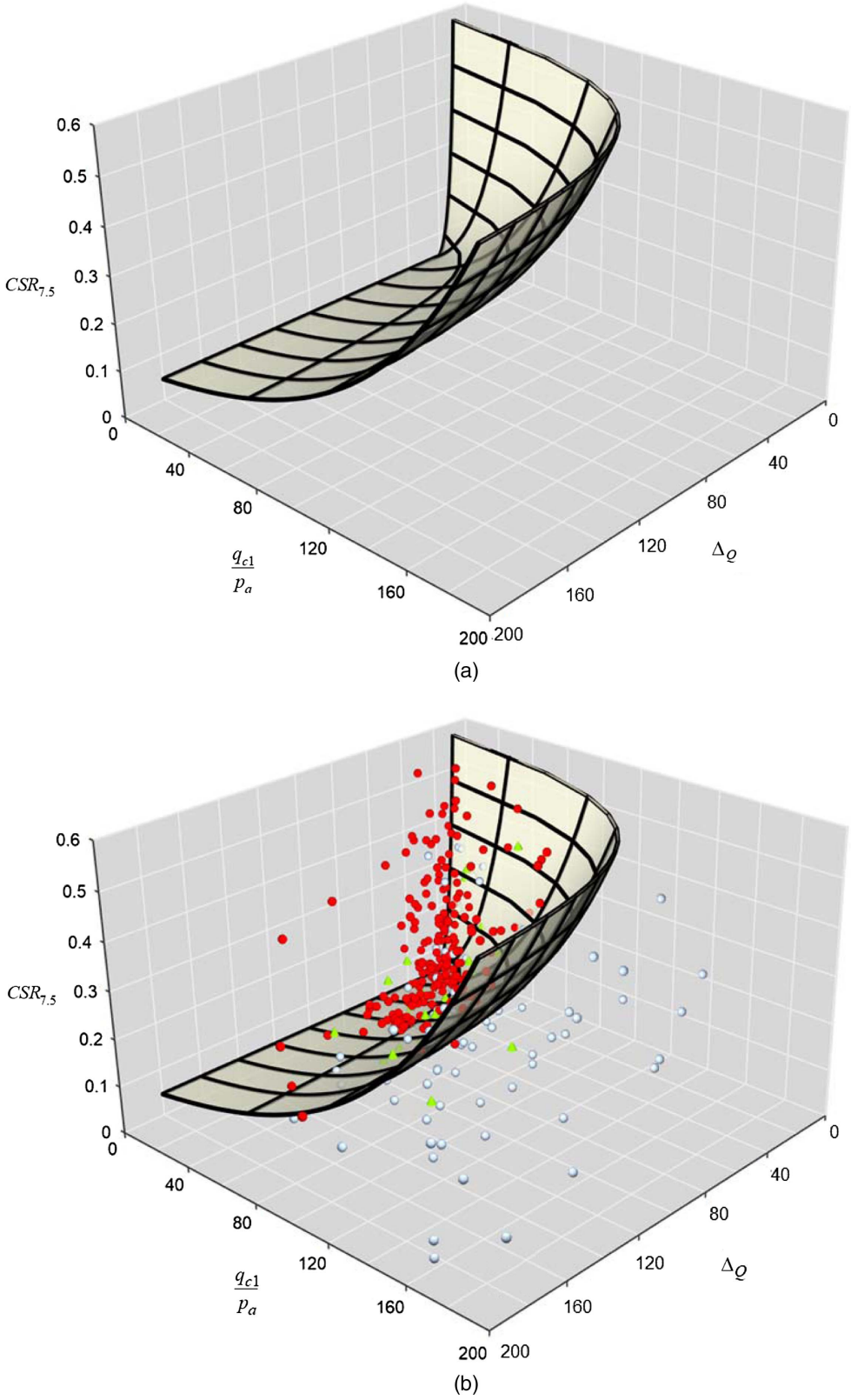

Fig. 6. Median (i.e., $P_L = 50\%$) $CRR_{7.5}$ liquefaction resistance boundary surface from Eq. (24) plotted in q_{c1}/p_a–$CSR_{7.5}$–Δ_Q space: (a) without and (b) with case history data.

where $\hat{m}_{CRR}$ is computed using Eq. (23) and X is an uncertainty term equal to $\sigma \cdot \Phi^{-1}[P_L]$. The term X therefore equals 0.092 if cone tip resistance for the soil and seismic loading are uncertain, or 0.077 if cone tip resistance for the soil and seismic loading ($CSR_{7.5}$) are assumed to be known with certainty. For typical geotechnical engineering projects, a value of $X = 0.092$ is recommended. With $CRR_{7.5}$ computed deterministically from Eq. (27), FS_{liq} can be computed using Eq. (25).

To understand why we recommend using the probabilistic *CRR* boundary surface corresponding to $P_L = 35\%$ as the deterministic liquefaction resistance boundary rather than the more traditional and widely accepted *CRR* boundary corresponding to $P_L = 15\%$, it is necessary to understand the relationship between P_L and FS_{liq} as it is computed from the median (i.e., best-fit) or $P_L = 50\%$ *CRR* boundary. In general, the following equation applies to all probabilistic liquefaction triggering relationships with uncertain input parameters:

$$P_L = \Phi\left[-\frac{\ln(FS_{liq,P_L=50\%})}{\sigma_{T,\ln}}\right] = \Phi\left[-\frac{\log(FS_{liq,P_L=50\%})}{\sigma_{T,\log}}\right] \quad (28)$$

where $FS_{liq,P_L=50\%}$ = factor of safety against liquefaction computed with the median or $P_L = 50\%$ *CRR* boundary; $\sigma_{T,\ln}$ = total standard deviation in natural log units; and $\sigma_{T,\log}$ = total standard deviation in logarithmic (base 10) units.

Boulanger and Idriss (2016) did not formally report a single regressed value of total standard deviation, $\sigma_{T,\ln}$ (which includes uncertainties in the input parameters, i.e., q_{c1}/p_a and $CSR_{7.5}$, as well as uncertainties in the model regression). Instead, they reported a recommended value of model standard deviation (i.e., assuming known and certain input parameters) of $\sigma_{\ln R} = 0.20$. If this model uncertainty value is substituted into Eq. (28) for $\sigma_{T,\ln}$, and a value of 15% is assigned to P_L, then a value of $FS_{liq,P_L=50\%} = 1.23$ is computed, which is intentionally conservative. However, re-regression of the Boulanger and Idriss (2016) liquefaction case history data set with their published model produces a value of $\sigma_{T,\ln} = 0.51$ (Arndt 2017). Interestingly, if this value of $\sigma_{T,\ln}$ is inserted into Eq. (28) with $FS_{liq,P_L=50\%} = 1.23$, a resulting value of $P_L = 34\%$ is computed.

Consider now the value of $\sigma_{T,\log} = 0.24$ for the Δ_Q common origin liquefaction resistance boundary introduced in this study. Inserting this value of $\sigma_{T,\log}$ into Eq. (28) with a value of $FS_{liq,P_L=50\%} = 1.24$ produces a value of $P_L = 35\%$, which is effectively the same as that computed with the Boulanger and Idriss (2016) model if $\sigma_{T,\ln}$ is used. We therefore emphasize that the deterministic $CRR_{7.5}$ boundary (with $P_L = 35\%$) recommended here actually corresponds to the same $FS_{liq,P_L=50\%}$ as other previously published liquefaction triggering relationships that recommend $P_L = 15\%$ for their deterministic $CRR_{7.5}$ boundaries.

It is common in engineering practice to incorporate an overall $FS_{liq} \geq 1.2$ to assess deterministically whether soils will (or will not) liquefy. When a deterministic liquefaction boundary corresponds to $P_L = 50\%$, it is appropriate to increase the assumed liquefaction triggering threshold in this manner to conservatively assess liquefaction. However, when a deterministic liquefaction resistance boundary is defined as $P_L < 50\%$, this boundary is inherently (and intentionally) conservative. In this study, the $CRR_{7.5}$ boundary corresponding to $P_L = 35\%$ is inherently conservative in that it already corresponds to $FS_{liq,P_L=50\%} = 1.24$, as described previously. Therefore, practitioners should define any additional increases in FS_{liq} and the assumed liquefaction resistance boundary based on the initial value of $FS_{liq,PL=50\%}$ and the desired level of conservatism required for a particular project.

Applications of Δ_Q Common-Origin Liquefaction Assessment

As discussed previously, the proposed Δ_Q common-origin liquefaction assessment provides a unified methodology to evaluate liquefaction susceptibility and triggering in CPT-compatible soils (from low-plasticity, nonsensitive fine-grained soils to coarse-grained soils). In the Supplemental Materials, we present several examples that illustrate the advantages of the proposed approach, using both deterministic and probabilistic analyses. For defining FS_{liq} below, we used the median ($P_L = 50\%$) liquefaction resistance boundary in the calculations. Therefore, as previously discussed, $FS_{liq} = 1.0$ corresponds to $P_L = 50\%$. The example field sites involve sites with clean sands, silty sands to sandy silts, and low-plasticity fine-grained soils. For brevity, we present two examples here—one that involved liquefaction-induced lateral spreading in both fine-grained and coarse-grained soils and one where liquefaction-induced silt boils were observed following the earthquake. We then illustrate the efficacy of the proposed Δ_Q common-origin liquefaction methodology for two particular subsets of the case history database: (1) the Darfield/Christchurch, New Zealand case records (Green et al. 2014), where other liquefaction triggering methods have been only moderately successful in forecasting the observed manifestations of liquefaction; and (2) cases involving fine-grained soils, where other liquefaction triggering methods (originally developed for coarse-grained soils) do not apply.

Example Applications from Moss Landing, California

Fig. 7 presents data from CPT UC-4, SPT boring UC B-10, and slope indicator SI-2 along Sandholdt Road at Moss Landing following the 1989 Loma Prieta earthquake ($M = 6.9$; Boulanger et al. 1997; Mejia 1998). As indicated by the inclinometer, liquefaction-induced lateral spreading occurred between depths of approximately 2 and 4.6 m. The adjoining channel bottom is near a depth of 5 m relative to the CPT UC-4 profile (Boulanger et al. 1997). Near the bottom of the zone of lateral displacement, Boulanger et al. (1997) identified an approximately 0.5-m-thick soft clayey silt unit (depth of about 3.7–4.2 m) sandwiched between units of poorly graded sand. The clayey silt unit exhibits $LL = 32$ and $I_P = 7$ (USCS = ML; $\Delta_Q \approx 25$–30), but is discontinuous at other areas of the site. Boulanger et al. (1997) also identified a 1.2-m-thick clayey silt unit (depth of about 4.6–5.8 m) just below the zone of lateral deformations with $LL = 46$ and $I_P = 21$ (USCS = CL; $\Delta_Q \approx 20$–30) in the upper portion and classified as ML in the lower portion. They suggested that the entire depth range from about 2 to 4.6 m liquefied, including both the sand and clayey silt units.

Figs. 7(d and e) present computed FS_{liq} with depth for CPT UC-4, indicating that the Δ_Q common-origin approach correctly forecasts liquefaction in the clayey silt units between the groundwater table and a depth of 6 m, with the channel base as well as the presence of denser sand (4.2–4.6 m) and higher plasticity soil (4.6–5 m) likely preventing significant lateral spreading of the clayey silt below a depth of 5 m. Specifically, the Δ_Q common-origin method forecasts liquefaction in the lower silty portion (5–5.8 m; $P_L > \sim 85\%$) of the clayey silt unit, but indicates that the upper clayey portion (~4.6–5 m) of the clayey silt unit is unlikely to liquefy ($P_L < \sim 10\%$). Higher calculated FS_{liq} ($P_L \approx 0\%$) below a depth of 6 m are consistent with the observations. However, only the uppermost portion (depth of about 2.1–2.3 m) of the deformed sand unit (depths of about 2.1–3.6 m) is predicted to be marginally liquefiable, with $q_{c1}/p_a \approx 85$–90, $\Delta_Q \approx 135$–140, $FS_{\text{liq}} \approx 1.0$–$1.5$, and $P_L \approx 25\%$–50%.

Similarly, Boulanger and Idriss (2016) identified multiple critical layers in this location: a zone of the deformed sand from depths of 2.0–3.0 m and the deeper undeformed sand from 6.0 to 10.0 m. These authors reported that the deformed sand exhibited an average $q_{c1}/p_a = 77$, although this depth range includes approximately 0.1 m of clayey soil (from depths of 2.0–2.1 m) and the CPT data indicate an average $q_{c1}/p_a = 133$ from 2.0 to 3.0 m (and

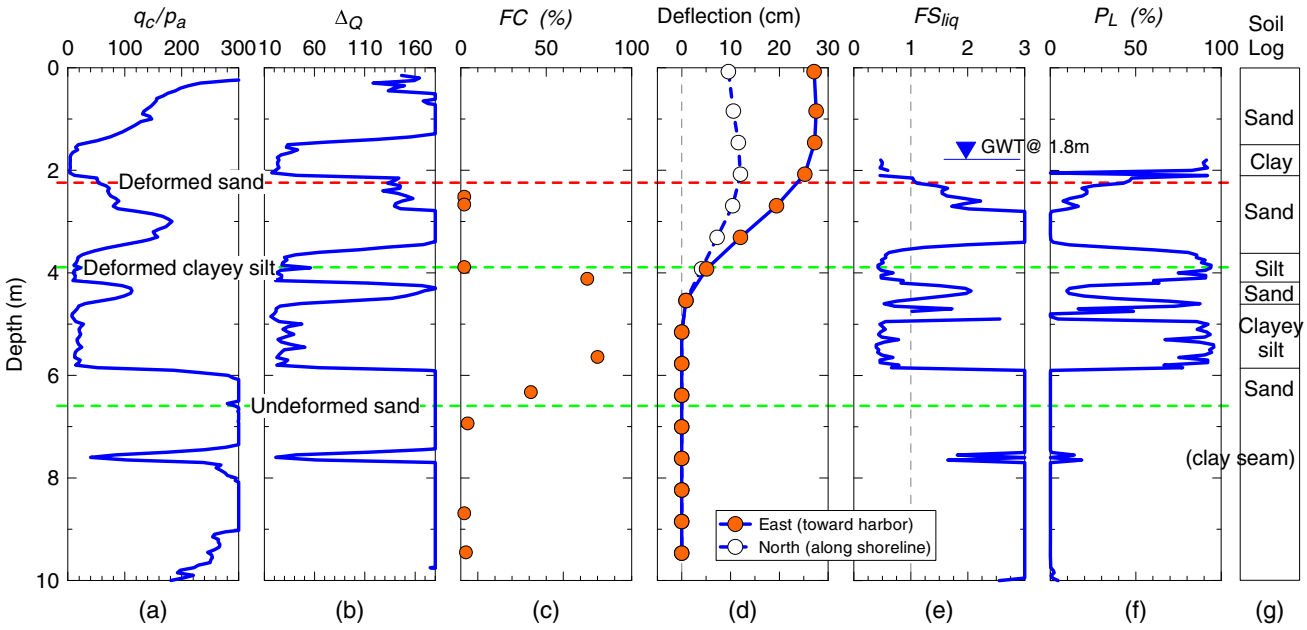

Fig. 7. Summary of Sandholdt Road site CPT sounding UC-4, adjacent SPT boring UC-B10, and adjacent slope indicator SI-2: (a) dimensionless tip resistance; (b) Δ_Q soil classification index; (c) fines content; (d) inclinometer deflections; (e) factor of safety against liquefaction using proposed Δ_Q common-origin method for 1989 Loma Prieta earthquake; (f) probability of liquefaction using proposed Δ_Q common-origin method for 1989 Loma Prieta earthquake; and (g) soil log. Included in the figure are the mid-depths of the critical layers (deformed sand, deformed clayey silt, and undeformed sand) used in this study.

$q_{c1}/p_a = 146$ from 2.1 to 3.0 m). The corresponding FS_{liq} using the Youd et al. (2001) procedure is approximately 0.6–12 from 2.1 to 3.0 m. Similar to the Δ_Q common-origin method, the cyclic stress method forecast $FS_{liq} \gg 1.0$ in the deeper undeformed sand. Importantly, Boulanger and Idriss (2016) did not include the clayey silt units in their database.

Similar to the Boulanger and Idriss (2016) analysis, Robertson and Wride (1998) reported that only the uppermost zone (depths of 2.1–2.7 m) was marginally liquefiable, while the remainder of the upper deformed sand (depths of 2.7–3.7 m) and the entire lower undeformed sand (depths of 5.8–10.1 m) exhibited $FS_{liq} \gg 1.0$. In contrast to the Δ_Q common-origin method, the Robertson and Wride (1998) cyclic stress method forecasts that zones from 3.8 to 4.2 m, 4.6 to 5.0 m, and 5.5 to 5.8 m of the clayey silt units are not susceptible to liquefaction.

During the 1989 Loma Prieta earthquake ($M = 6.9$), the Moss Landing Marine Laboratory (MLML) was also damaged beyond repair (Boulanger et al. 1997; Mejia 1998) as a result of liquefaction-induced lateral spreading. Of particular interest at the MLML was the formation of a fine-grained clayey silt boil in the volleyball court near the southeast corner of the site. Fig. 8 presents data from CPT C-3, SPT borings UC-7 and JB-2, and test pit TP-A, which were performed near the silt boil. Mejia (1998) indicated that numerous clayey silt vents were encountered in the 2.4-m-deep test pit, suggesting that the "silt flowed to the surface in a liquefied state." Samples from the silt boil exhibited an average $w_L \approx 38$, $I_P \approx 17$, $FC \approx 78$, and clay fraction (percent smaller than 5 μm) ≈ 24. Based on these observations, Boulanger et al. (1997) concluded that liquefaction occurred in both the clayey silt unit and the uppermost loose to medium-dense portion of the beach sand unit, although they did not list the clayey silt unit as having experienced liquefaction or cyclic softening.

In this study, we considered the entire clayey silt unit (below the groundwater table) from depths of 1.5–4.0 m as the critical layer to be consistent with the silt boil observed at the site. As shown in Fig. 8, this unit generally exhibited $\Delta_Q \approx 20$–40, $FS_{liq} \approx 0.4$–0.6, and $P_L \approx 85\%$–95%, consistent with the observed lateral spread and clayey silt boil. Only a thin zone of looser sand (depths of about 4.0–4.5 m) at the top of the sand unit underlying the clayey silt was forecast to liquefy using the Δ_Q common-origin method. This thin zone of liquefiable sand would be unlikely to liquefy the overlying clayey silt via porewater and porewater pressure redistribution or to create, via erosion and entrainment with fluidized sand, the silt boils observed at the surface.

Christchurch/Darfield, New Zealand Sites

Green et al. (2014) presented CPT data for 25 sites that were subjected to the 2010 Darfield (M7.1) and 2011 Christchurch (M6.2), New Zealand, earthquakes. These 25 sites were selected because many of them involved minor (i.e., marginal) liquefaction manifestations or experienced liquefaction during one of the earthquakes and did not liquefy during the other earthquake. In addition, the 25 sites selected by Green et al. had relatively well-constrained ground motions as well as CPT and surface wave geophysical data available. Unfortunately, the CPT sleeve friction readings were highly suspect at site RCH-14 (nearly all recorded f_s values were practically zero), resulting in the sounding being unusable for this study. Discounting this site, the Green et al. (2014) data set yielded 48 usable case records.

Fig. 9 presents the New Zealand data set in Δ_Q-m_{CSR} space. As illustrated in the figure, all liquefaction cases classify correctly and all but one of the nonliquefaction cases classify correctly (or plot on the m_{CRR} boundary) with respect to the median (50th percentile) m_{CRR} liquefaction resistance boundary. However, 6 of 18 marginal cases are misclassified in the nonliquefaction region (with one of those six nearly on the line). The one nonliquefaction and six

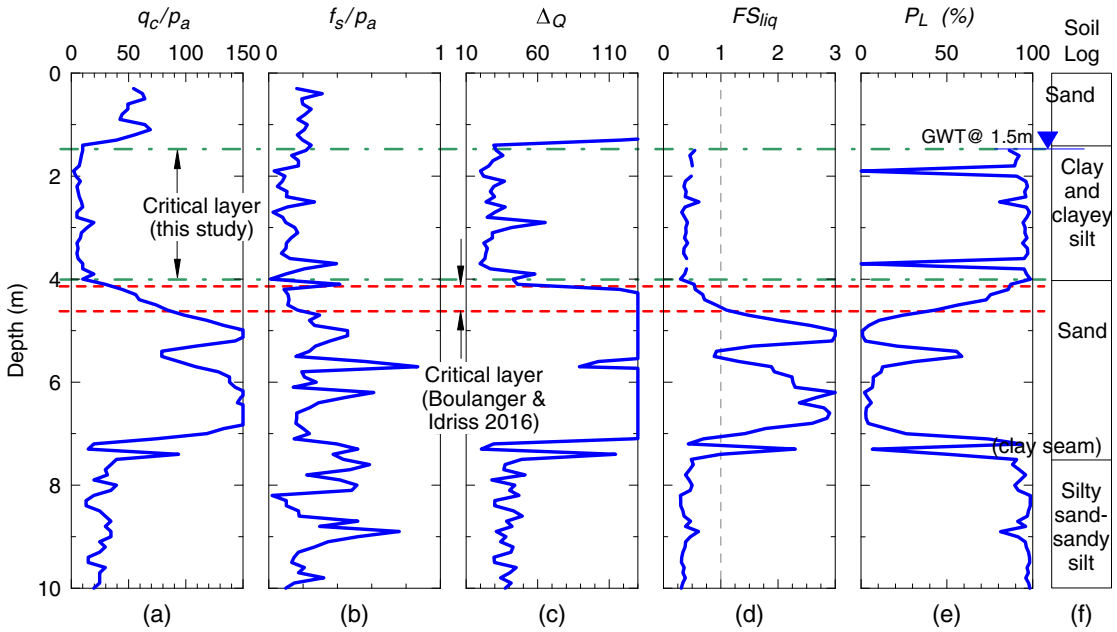

Fig. 8. Summary of MLML site CPT sounding C-3, adjacent SPT boring UC-7, and test pit TP-A: (a) dimensionless tip resistance; (b) dimensionless sleeve friction; (c) Δ_Q soil classification index; (d) factor of safety against liquefaction using proposed Δ_Q common-origin method for 1989 Loma Prieta earthquake; (e) probability of liquefaction using proposed Δ_Q common-origin method for 1989 Loma Prieta earthquake; and (f) soil log. Included in the figure are the critical layers used by Boulanger and Idriss (2016) and in this study.

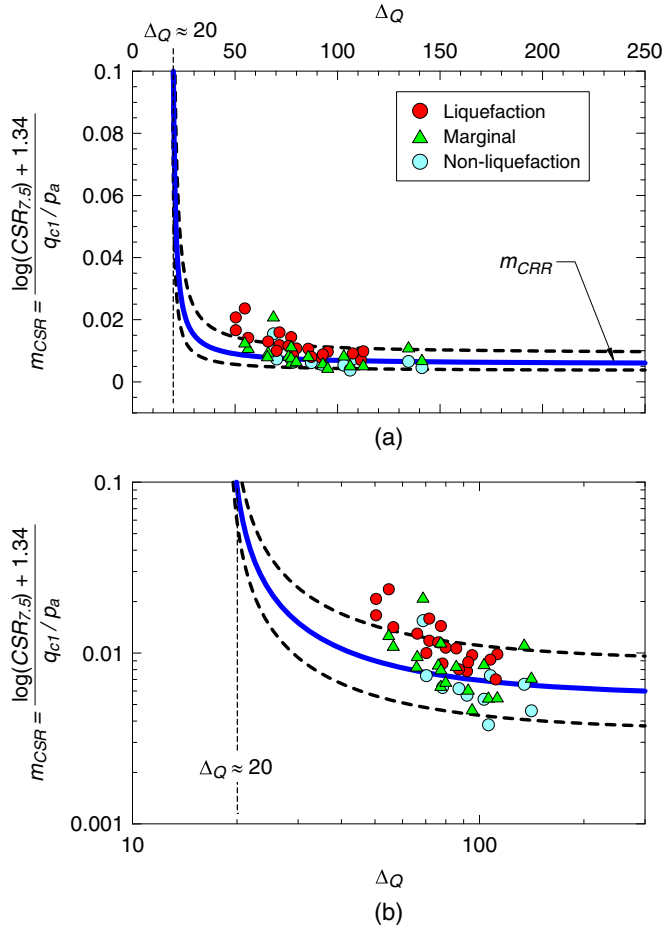

Fig. 9. Liquefaction case histories for 2010 Darfield and 2011 Christchurch, New Zealand, earthquakes plotted in m_{CSR}-Δ_Q space: (a) arithmetic scale; and (b) log-log scale.

marginal liquefaction cases that are misclassified represent only 15% of the New Zealand data set presented here.

Fine-Grained Soil Case Histories

Moss et al. (2006) suggested that while low-plasticity, fine-grained soils are not susceptible to sandlike liquefaction, these soils can experience cyclic softening and shear failure and can produce observable liquefaction-like ground failures, including building tilting, punching, and settlement that are similar to ground failures observed in nonplastic, coarse-grained soils. However, in some cases such as the aforementioned MLML, low-plasticity silty and clayey soils have manifest fluidization features including subsurface dikes (vents) and surface boils, which often are presumed to occur only in sandy soils. Currently, screening-level assessment of liquefaction susceptibility in nonsensitive, fine-grained soil involves using index properties including Atterberg limits, water content, and clay fraction (e.g., Youd et al. 2001; Seed et al. 2003; Boulanger and Idriss 2004, 2006; Bray and Sancio 2006; among others). If the soil is susceptible to liquefaction, these (and similar) approaches commonly recommend retrieving high-quality undisturbed samples and performing laboratory cyclic testing to assess the potential for liquefaction triggering.

The Robertson and Wride (1998) liquefaction triggering approach suggests that soils with $I_c > 2.6$ are not susceptible to sandlike liquefaction. However, Table S1 includes a number of liquefied sites with soils that exhibit $I_c > 2.6$. To investigate these cases, Fig. 10 presents all the cases in Table S1 with $\Delta_Q \leq 31$, which corresponds (on average) to $FC \approx 50\%$ (Saye et al. 2017). Fig. 10 includes the relationships for $\Delta_Q = 19$ and 21. These liquefaction and nonliquefaction data and the comparisons to I_c and Δ_Q suggest that $\Delta_Q \approx 20$ is a reasonable threshold to identify nonsensitive, fine-grained soils that are susceptible to significant cyclic softening and liquefaction-like behavior. That is, the Δ_Q common-origin approach essentially couples the index property-based liquefaction susceptibility analysis (as proposed by others) with the CPT-based

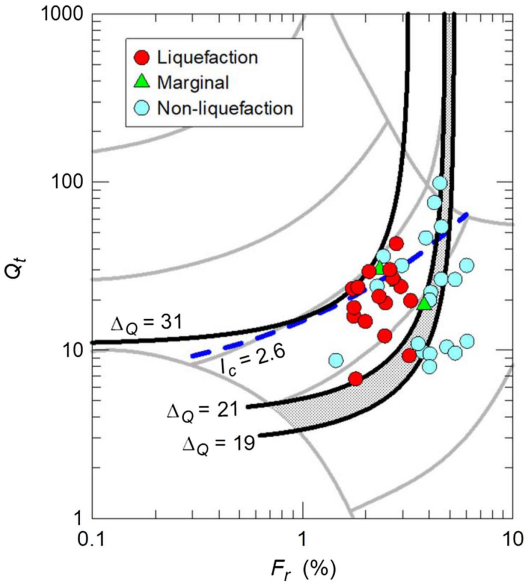

Fig. 10. Liquefaction case histories involving fine-grained soils with $\Delta_Q \leq 31$ plotted in $Q_t - F_r$ space. Included in the plot are the Robertson (1990) soil behavior type boundaries, the soil behavior type index, $I_c = 2.6$ boundary, as well as a shaded region between $\Delta_Q = 19$ and 21.

triggering analysis for low-plasticity, nonsensitive fine-grained soils. This is illustrated previously using examples at Moss Landing during the 1989 Loma Prieta earthquake and additional examples in the Supplemental Materials.

Conclusions

In this study, we compiled and consistently interpreted 401 documented case records of liquefaction and nonliquefaction in clean sands, silty sands, sandy silts, and low-plasticity, nonsensitive fine-grained soils to develop a new procedure to simultaneously assess liquefaction susceptibility and level-ground liquefaction triggering for CPT-compatible soils ranging from nonsensitive clays to clean sands using the soil classification index, Δ_Q (Saye et al. 2017). The new procedure is based on the concept of a common origin, which is defined as the y-axis intercept (c_o) for liquefaction resistance boundaries when the boundaries are plotted in $\log_{10} CSR_{7.5}$–q_{c1}/p_a space. The slopes of the boundaries are defined as m_{CRR} in $\log_{10} CSR_{7.5}$–q_{c1}/p_a space, which can be related to soil index properties and Δ_Q.

Using Bayesian maximum likelihood regression, a probabilistic Δ_Q common-origin model was created. The probabilistic regression indicates a threshold of $\Delta_Q \geq 20$ for soils to be susceptible to liquefaction or significant cyclic softening. Based on soil index property data presented by Saye et al. (2017), this threshold of $\Delta_Q \approx 20$ corresponds approximately to a liquid limit of about 30%–40%, plasticity index of about 15%–20%, and D_{50} of about 0.03 mm. This Δ_Q value marks a change between low-plasticity, nonsensitive fine-grained soils susceptible to level-ground liquefaction and medium-plasticity, nonsensitive fine-grained soils and organic soils not susceptible to liquefaction.

Coupled with the simplified equation to estimate cyclic stress ratio (Seed and Idriss 1971; Whitman 1971), adjusted for earthquake moment magnitude, $CSR_{7.5}$, the Δ_Q common-origin method can be used to estimate a factor of safety against liquefaction (FS_{liq}) and/or a probability of liquefaction (P_L). Assuming a value of $P_L = 35\%$ consistent with standard engineering practice today, a deterministic Δ_Q common-origin model also was created and presented. This deterministic boundary corresponds to an equivalent FS_{liq} of approximately 1.24 (relative to the median cyclic resistance boundary, i.e., $P_L = 50\%$). Therefore, when used for design, any additional factor of safety should be defined based on the desired level of conservatism needed for an individual project.

The proposed probabilistic and deterministic Δ_Q common-origin method (1) eliminates the need for a fines-content adjustment to adjust the CPT tip resistance measured in silty sands to an equivalent clean-sand CPT tip resistance; (2) incorporates case histories involving low-plasticity, nonsensitive fine-grained soils into the database and, in doing so, extends and unifies the evaluation of liquefaction susceptibility and triggering for coarse-grained and low-plasticity, nonsensitive fine-grained soils; and (3) differentiates the liquefaction resistance of clean sands based on CPT measurements (which reflect properties such as compressibility and mineralogy) rather than treating all clean sands identically. These advantages are illustrated using a series of example applications for cases of liquefaction, marginal liquefaction, and no liquefaction in clean sands, silty sands to sandy silts, and low-plasticity fine-grained soils.

Data Availability Statement

Some or all data, models, or code that support the findings of this study are available from the corresponding author upon reasonable request. Some or all data, models, or code used during the study were provided by Prof. Johann Facciorusso. Direct request for these materials may be made to Prof. Facciorusso as indicated in the Acknowledgments.

Acknowledgments

The authors would like to acknowledge and thank the following individuals for their contributions to this work: Prof. Bret Lingwall for discussions related to universal liquefaction resistance concepts; Prof. Johann Facciorusso for sharing digital CPT data collected following the 2015 Emilia, Italy, earthquake; and Mr. Ryan Leigh for his initial compilation and review of CPT data. The authors also thank the anonymous reviewers for their insightful comments, which helped the authors improve the manuscript.

Supplemental Materials

Tables S1–S5, Figs. S1–S10, and Eqs. (S1)–(S33) are available online in the ASCE Library (www.ascelibrary.org).

References

Ajmera, B., T. Brandon, and B. Tiwari. 2019. "Characterization of the reduction in undrained shear strength in fine-grained soils due to cyclic loading." *J. Geotech. Geoenviron. Eng.* 145 (5): 10. https://doi.org/10.1061/(ASCE)GT.1943-5606.0002041.

Arndt, A. M. 2017. "Performance-based liquefaction triggering analyses with two liquefaction models using cone penetration test." M.S. thesis, Dept. of Civil and Environmental Engineering, Brigham Young Univ.

Bennett, M. J., and J. C. Tinsley III. 1995. *Geotechnical data from surface and subsurface samples outside of and within liquefaction-related ground failures caused by the October 17, 1989, Loma Prieta*

earthquake, Santa Cruz and Monterey counties, California. Open-file Rep. 95-663. Washington, DC: USGS, US Dept. of the Interior.
Boulanger, R. W., and I. M. Idriss. 2004. *Evaluating the potential for liquefaction or cyclic failure of silts and clays.* Rep. No. UCD/CGM-04/01. Davis, CA: Univ. of California.
Boulanger, R. W., and I. M. Idriss. 2006. "Liquefaction susceptibility criteria for silts and clays." *J. Geotech. Geoenviron. Eng.* 132 (11): 1413–1426. https://doi.org/10.1061/ASCE1090-02412006132:111413.
Boulanger, R. W., and I. M. Idriss. 2012. "Probabilistic standard penetration test-based liquefaction-triggering procedure." *J. Geotech. Geoenviron. Eng.* 138 (10): 1185–1195. https://doi.org/10.1061/(ASCE)GT.1943-5606.0000700.
Boulanger, R. W., and I. M. Idriss. 2014. *CPT and SPT based liquefaction triggering procedures*. Rep. No. UCD/CGM-14/01. Davis, CA: Univ. of California.
Boulanger, R. W., and I. M. Idriss. 2016. "CPT-based liquefaction triggering procedure." *J. Geotech. Geoenviron. Eng.* 142 (2): 11. https://doi.org/10.1061/(ASCE)GT.1943-5606.0001388.
Boulanger, R. W., L. H. Mejia, and I. M. Idriss. 1997. "Liquefaction at moss landing during Loma Prieta earthquake." *J. Geotech. Geoenviron. Eng.* 123 (5): 453–467. https://doi.org/10.1061/(ASCE)1090-0241(1997)123:5(453).
Box, G. E. P., and G. C. Tiao. 1973. *Bayesian inference in statistical analysis*. Boston, MA: Addison-Wesley Publishing Company.
Bray, J. D., and R. B. Sancio. 2006. "Assessment of the liquefaction susceptibility of fine-grained soils." *J. Geotech. Geoenviron. Eng.* 132 (9): 1165–1177. https://doi.org/10.1061/(ASCE)1090-0241(2006)132:9(1165).
Cetin, K. O., A. Der Kiureghian, and R. B. Seed. 2002. "Probabilistic models for the triggering of seismic soil liquefaction." *Struct. Saf.* 24 (1): 67–82. https://doi.org/10.1016/S0167-4730(02)00036-X.
Cetin, K. O., R. B. Seed, A. Der Kiureghian, K. Tokimatsu, L. F. Harder Jr., R. E. Kayen, and R. E. S. Moss. 2004. "SPT-based probabilistic and deterministic assessment of seismic soil liquefaction potential." *J. Geotech. Geoenviron. Eng.* 130 (12): 1314–1340. https://doi.org/10.1061/(ASCE)1090-0241(2004)130:12(1314).
Charlie, W. A., D. O. Doehring, J. P. Brislawn, and H. Hassen. 1998. "Direct measurement of liquefaction potential in soils of Monterey County, California." In *The Loma Prieta, California, earthquake of October 17, 1989—Liquefaction*, edited by T. L. Holzer, 181–221. Washington, DC: USGS.
Der Kiureghian, A. 1999. "A Bayesian framework for fragility assessment." In *Proc., ICASP8 Conf., Int. Civil Engineering Risk and Reliability Association*, 1003–1010. Rotterdam, Netherlands: A.A. Balkema.
Green, R. A., M. Cubrinovski, B. Cox, C. Wood, L. Wotherspoon, B. Bradley, and B. Maurer. 2014. "Select liquefaction case histories from the 2010–2011 Canterbury earthquake sequence." *Earthquake Spectra* 30 (1): 131–153. https://doi.org/10.1193/030713EQS066M.
Green, R. A., S. F. Obermeier, and S. M. Olson. 2005. "Engineering geologic and geotechnical analysis of paleoseismic shaking using liquefaction effects: Field examples." *Eng. Geol.* 76 (3–4): 263–293. https://doi.org/10.1016/j.enggeo.2004.07.026.
Idriss, I. M., and R. W. Boulanger. 2008. "Soil liquefaction during earthquakes." In *Monograph MNO-12*. Oakland, CA: Earthquake Engineering Research Institute.
Ishihara, K. 1985. "Stability of natural deposits during earthquakes." In Vol. 1 of *Proc., 11th Int. Conf. on Soil Mechanics and Foundation Engineering*, 321–376. London: International Society for Soil Mechanics and Geotechnical Engineering.
Kayen, R., R. E. S. Moss, E. M. Thompson, R. B. Seed, K. O. Cetin, A. Der Kiureghian, Y. Tanaka, and K. Tokimatsu. 2013. "Shear-wave velocity-based probabilistic and deterministic assessment of seismic soil liquefaction potential." *J. Geotech. Geoenviron. Eng.* 119 (3): 407–419. https://doi.org/10.1061/(ASCE)GT.1943-5606.0000743.
Liao, S. S. C., and K. Y. Lum. 1998. "Statistical analysis and application of the magnitude scaling factor in liquefaction analysis." In *Proc., Geotechnical Earthquake Engineering and Soil Dynamics III*, 410–421. Reston, VA: ASCE.
Liao, S. S. C., D. Veneziano, and R. V. Whitman. 1988. "Regression models for evaluating liquefaction probability." *J. Geotech. Eng.* 114 (4): 389–409. https://doi.org/10.1061/(ASCE)0733-9410(1988)114:4(389).
Manski, C. F., and S. R. Lerman. 1977. "The estimation of choice probabilities from choice-based samples." *Econometrica* 45 (8): 1977–1998. https://doi.org/10.2307/1914121.
Mejia, L. H. 1998. "Liquefaction at Moss Landing." In *The Loma Prieta, California, Earthquake of October 17, 1989—Liquefaction*, edited by T. L. Holzer, 129–150. Washington, DC: USGS.
Moss, R. E. S., R. B. Seed, R. E. Kayen, J. P. Stewart, A. Der Kiureghian, and K. O. Cetin. 2006. "CPT-based probabilistic and deterministic assessment of in situ seismic soil liquefaction potential." *J. Geotech. Geoenviron. Eng.* 132 (8): 1032–1051. https://doi.org/10.1061/(ASCE)1090-0241(2006)132:8(1032).
National Academies of Sciences, Engineering, and Medicine. 2016. *State of the art and practice in the assessment of earthquake-induced soil liquefaction and its consequences*. Washington, DC: National Academies Press.
Olson, S. M., R. A. Green, and S. F. Obermeier. 2005. "Geotechnical analysis of paleoseismic shaking using liquefaction features: A major updating." *Eng. Geol.* 76 (3–4): 235–261. https://doi.org/10.1016/j.enggeo.2004.07.008.
Robertson, P. K. 1990. "Soil classification by the cone penetration test." *Can. Geotech. J.* 27 (1): 151–158. https://doi.org/10.1139/t90-014.
Robertson, P. K. 2009. "Interpretation of cone penetration tests—A unified approach." *Can. Geotech. J.* 46 (11): 1337–1355. https://doi.org/10.1139/T09-065.
Robertson, P. K., and K. L. Cabal. 2015. *Guide to cone penetration testing for geotechnical engineering*. 6th ed., 133. Signal Hill, CA: Gregg Drilling and Testing.
Robertson, P. K., and R. G. Campanella. 1983. "Interpretation of cone penetration tests—Part I (sand)." *Can. Geotech. J.* 20 (4): 718–733. https://doi.org/10.1139/t83-078.
Robertson, P. K., and R. G. Campanella. 1985. "Liquefaction potential of sand using the CPT." *J. Geotech. Eng.* 111 (3): 384–403. https://doi.org/10.1061/(ASCE)0733-9410(1985)111:3(384).
Robertson, P. K., and C. E. Wride. 1998. "Evaluating cyclic liquefaction potential using the cone penetration test." *Can. Geotech. J.* 35 (3): 442–459. https://doi.org/10.1139/t98-017.
Saye, S. R., J. Santos, S. M. Olson, and R. D. Leigh. 2017. "Linear trendlines to assess soil classification from cone penetration tests." *J. Geotech. Geoenviron. Eng.* 143 (9): 15. https://doi.org/10.1061/(ASCE)GT.1943-5606.0001729.
Seed, H. B., and P. de Alba. 1986. "Use of SPT and CPT tests for evaluating the liquefaction resistance of sands." In *Use of in situ tests in geotechnical engineering*, 281–302. Reston, VA: ASCE.
Seed, H. B., and I. M. Idriss. 1971. "Simplified procedure for evaluation soil liquefaction potential." *J. Soil Mech. Found. Div.* 97 (9): 1249–1273.
Seed, H. B., and I. M. Idriss. 1982. "Ground motions and soil liquefaction during earthquakes." In *Monograph series*, 134. Oakland, CA: Earthquake Engineering Research Institute.
Seed, H. B., K. Tokimatsu, L. F. Harder, and R. M. Chung. 1985. "Influence of SPT procedures in soil liquefaction resistance evaluations." *J. Geotech. Eng.* 111 (12): 1425–1445. https://doi.org/10.1061/(ASCE)0733-9410(1985)111:12(1425).
Seed, R. B., et al. 2003. *Recent advances in soil liquefaction engineering: A unified and consistent framework.* EERC-2003-06. Berkeley, CA: Earthquake Engineering Research Institute.
Stark, T. D., and S. M. Olson. 1995. "Liquefaction resistance using CPT and field case histories." *J. Geotech. Eng.* 121 (12): 856–869. https://doi.org/10.1061/(ASCE)0733-9410(1995)121:12(856).
Whitman, R. V. 1971. "Resistance of soil to liquefaction and settlement." *Soils Found.* 11 (4): 59–68. https://doi.org/10.3208/sandf1960.11.4_59.
Youd, T. L., et al. 2001. Liquefaction resistance of soils: Summary report from the 1996 NCEER and 1998 NCEER/NSF workshops on evaluation of liquefaction resistance of soils." *J. Geotech. Geoenviron. Eng.* 127 (10): 817–833. https://doi.org/10.1061/(ASCE)1090-0241(2001)127:10(817).
Youd, T. L., and S. K. Noble. 1997. "Liquefaction criteria based on statistical and probabilistic analyses." In *Proc., NCEER Workshop on Evaluation of Liquefaction Resistance of Soils*, 201–205. Alexandria, VA: National Science Foundation.